Nano Research

ISSN 1998-0124 CN 11-5974/O4
https://doi.org/10.1007/s12274-023-5818-4

Research Article

Lateral dipole moments induced by all-*cis*-pentafluorocyclohexyl groups cause unanticipated effects in self-assembled monolayers

Christian Fischer[1], Saunak Das[2], Qingzhi Zhang[3], Yangbiao Liu[2], Lothar Weinhardt[4,5,6], David O'Hagan[3] (✉), Michael Zharnikov[2] (✉), and Andreas Terfort[1] (✉)

[1] *Institute of Inorganic and Analytical Chemistry, Goethe University Frankfurt, Max-von-Laue-Straße 7, 60438 Frankfurt am Main, Germany*
[2] *Applied Physical Chemistry, Heidelberg University, Im Neuenheimer Feld 253, 69120 Heidelberg, Germany*
[3] *School of Chemistry, University of St Andrews, North Haugh, St Andrews, Fife, KY16 9ST, UK*
[4] *Institute for Photon Science and Synchrotron Radiation, Karlsruhe Institute of Technology (KIT), Hermann-v.-Helmholtz-Platz 1, 76344 Eggenstein-Leopoldshafen, Germany*
[5] *Institute for Chemical Technology and Polymer Chemistry (ITCP), Karlsruhe Institute of Technology (KIT), Engesserstr. 18/20, 76128 Karlsruhe, Germany*
[6] *Department of Chemistry and Biochemistry, University of Nevada, Las Vegas (UNLV), 4505 Maryland Parkway, Las Vegas, NV 89154-4003, USA*

Received: 3 March 2021 / **Revised:** 30 April 2023 / **Accepted:** 7 May 2023

ABSTRACT

All-*cis*-hexafluoro- and all-cis-pentafluoro-cyclohexane (PFCH) derivatives are new kinds of materials, the structures and properties of which are dominated by the highly dipolar Janus-face motif. Here, we report on the effects of integrating the PFCH groups into self-assembled monolayers (SAMs) of alkanethiolates on Au(111). Monolayers with an odd (eleven) and even (twelve) number of methylene groups were characterized in detail by several complementary experimental tools, supported by theoretical calculations. Surprisingly, all the data show a high similarity of both kinds of monolayers, nearly lacking the typically observed odd-even effects. These new monolayers have a packing density about 1/3 lower than that of non-substituted alkanethiolate monolayers, caused by the bulkiness of the PFCH moieties. The orientations of the PFCH groups and the alkyl chains could be determined independently, suggesting a conformation similar to the one found in the solid state structure of an analogous compound. Although in the SAMs the PFCH groups are slightly tilted away from the surface normal with the axial fluorine atoms pointing downwards, most of the dipole moments of the group remain oriented parallel to the surface, which is a unique feature for a SAM system. The consequences are much lower water contact angles compared to other partly fluorinated SAMs as well as rather moderate work function values. The interaction between the terminal PFCH moieties results in an enhanced stability of the PFCH-decorated SAMs toward exchange reaction with potential molecular substituents in spite of the lower packing density of these films.

KEYWORDS

odd-even-effects, work function, self-assembled monolayer (SAM), kinetic stability, infrared-reflection absorption spectroscopy, X-ray photoelectron spectroscopy

1 Introduction

Perfluorinated and partly fluorinated molecules are of significant interest in the fields of material science, agrochemistry and medicinal chemistry [1–3]. While perfluorinated compounds are typically obtained by exhaustive fluorination [4, 5], partially fluorinated motifs have gained more popularity recently as advances in synthetic chemistry now permit good control over substitution patterns [6, 7]. Due to the strong polarization of the C–F bonds, partly fluorinated molecules often exhibit strong molecular dipole moments, in particular in combination with rigid molecular conformations [8, 9]. An extreme example is the Janus-faced all-*cis* 1,2,3,4,5,6-hexafluorocyclohexane (HFCH), which displays an extraordinarily high dipole moment of 6.5 D across its two faces (hydrogen face and fluorine face). In the solid phase, this causes an extended stability with strong stacking between molecular layers and a high melting point of 208 °C [10]. The first synthesis of HFCH was reported in 2015 by Keddie et al. [10] starting from myo-inositol, which was converted to HFCH in a lengthy 12 step synthesis with low yields. In 2017, Glorius et al. [11] developed a new route starting from hexafluorobenzene using Zeng's cyclic (alkyl)(amino)carbene (CAAC)/rhodium catalyst [12] as a hydrogenation catalyst for the *cis*-selective synthesis of fluorinated cycloalkanes. This shortens the synthesis to a single step, providing easy access to this class of molecules. The new route further tolerates several functional groups, enabling access to mono-substituted all-*cis* 2,3,4,5,6-pentafluorocyclohexane (PFCH) derivatives for new applications, such as the solution state coordination of anions [13] and the controlled supramolecular assembly of polymers [14]. Furthermore, the syntheses of derivatives for application in medicinal chemistry have been explored [15, 16].

Address correspondence to David O'Hagan, do1@st-andrews.ac.uk; Michael Zharnikov, Michael.Zharnikov@urz.uni-heidelberg.de; Andreas Terfort, aterfort@chemie.uni-frankfurt.de

The mono-alkylated PFCH derivatives adopt an interesting conformation, in which the alkyl substituent lies preferably in the equatorial position, resulting in three axial C–F bonds instead of an axially oriented alkyl chain and two axial C–F bonds [17, 18] This is unexpected as this conformation leads to increased polarity of the resulting material, but is supported by both computational studies and analysis of solid-state structures, conducted by Clark et al. [17]. Presumably the reason for this interesting conformation is a combination of strong dipole–dipole interactions and additional H···F interactions between neighboring molecules resulting in a higher stability of the observed arrangement. We figured that such strong interactions might also lead to improved packing within self-assembled monolayers (SAMs), increasing the stability of the SAMs.

Several dipolar SAMs have been reported in the literature before [19, 20], and for many of those, fluorine atoms or fluorine-containing groups, such as the trifluoromethyl [21] or pentafluorosulfanyl group [22], have been used to introduce the dipole moments. Significantly, in all these cases, the dipole moments were oriented along the molecular axis and, consequently, nearly perpendicular to the substrate (upright molecular orientation), which has a strong influence on such properties as the work function but not so much on the stability of the SAM. In the case of the PFCH headgroup, the dipole moment of the SAM-forming molecules should be oriented almost perpendicular to the molecular axis, providing a unique opportunity to study its effect for this specific orientation.

Starting from previously reported derivatives of the PFCH moiety with long ω-alkanol side chains [17], suitable anchoring groups should be introduced, such as thiol groups for the deposition onto gold surfaces. As it is known that the parity of the number of methylene groups in the alkyl chains can play a role in the properties of the resulting films (odd-even effect), we decided to prepare the derivative with eleven CH_2 groups (odd) as well as the one with twelve CH_2 groups (even), see Fig. 1. The resulting SAMs were thoroughly investigated in particular regarding their structural quality as well as the orientation of the molecular subunits.

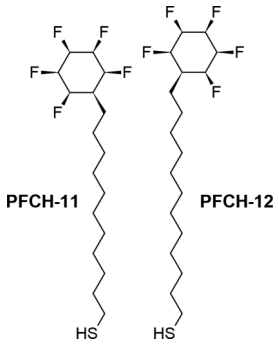

Figure 1 The SAM-forming molecules of the present study along with their acronyms (PFCH-*n* for both molecules). The expected influence of the parity of the number of CH_2 groups on the orientation of the PFCH tail groups is clearly visible.

2 Experimental section

Synthesis of SAM precursors. The long chain thiols PFCH-11 and PFCH-12 were prepared by extending the previously reported synthesis of long chain fatty methyl esters carrying terminal PFCH rings, to the corresponding thiols [16]. The route to the desired thiols is summarized in Scheme 1.

Substrates. The gold substrates were prepared in-house in ultra-high vacuum (UHV) by thermal evaporation of 5 nm Ti (adhesive layer) followed by 200 nm Au onto commercial 6-inch Si(100) wafers. The resulting films were polycrystalline, exposing mostly (111) orientated surfaces of individual crystallites.

Monolayer preparation. Substrates were freshly cut into 1 cm × 2 cm pieces, rinsed with ethanol (p.a. grade) and cleaned in hydrogen-plasma [23] (0.5 mbar) for 2 min. For ellipsometry, the substrate parameters were measured at this stage. The PFCH-*n* SAMs were prepared by immersion of the freshly prepared substrates in solutions of the respective precursors in spectroscopic grade ethanol (0.1 mM, 24 h, room temperature). Subsequently, the SAMs were thoroughly washed with ethanol and dried in a stream of Ar or nitrogen. In addition, hexadecanethiolate (C16), dodecanethiolate (C12), and perdeuterated dodecanethiolate (C12-D) SAMs were prepared on similar gold substrates as references. The monolayer samples were either characterized immediately after the preparation or kept in nitrogen-filled containers until spectroscopic characterization.

Ellipsometry. Measurements were carried out with a Sentech SE 400 ellipsometer equipped with a He-Ne laser with a wavelength of 632.8 nm and a beam diameter of 1–2 mm at an angle of incidence of 70° with respect to the surface normal. For each substrate four different spots were measured. The extinction coefficients of the SAMs were assumed to be zero and the real part of the refractive indices was set to 1.55 for all measurements.

X-ray spectroscopy. The SAMs were characterized by synchrotron-based X-ray photoelectron spectroscopy (XPS) and near-edge X-ray absorption fine structure (NEXAFS) spectroscopy. The experiments were carried out at the HE-SGM beamline of the synchrotron storage ring BESSY II in Berlin. The experimental station featured a Scienta R3000 electron energy analyzer and a custom-designed partial electron yield (PEY) detector [24]. The measurements were performed at room temperature and under ultra-high vacuum conditions. The photon flux provided by the beamline (bending magnet) was rather moderate, but the spectra acquisition time was kept reasonably short to avoid any modification of the monolayers by X-rays, which is particularly important for radiation-sensitive fluorinated SAMs [25, 26]. No characteristic features of such a modification were recorded in the spectra.

XPS. The XPS spectra were acquired in normal emission geometry. Photon energy (PE) of the primary X-ray beam was varied between 350 and 750 eV depending on the particular spectral range. The binding energy (BE) scale of the spectra was referenced to the Au $4f_{7/2}$ peak of the gold substrate at 84.0 eV [27]. The energy resolution was ~ 0.3 eV at a PE of 350 eV and progressively lower at the higher PEs. The spectra were fitted by symmetric Voigt functions and a linear background. The S $2p_{3/2,1/2}$ doublets were fitted by a combination of two Voigt peaks with the same Gaussian and Lorentzian widths, a branching ratio of 2, and a spin–orbit splitting of ~ 1.18 eV [27].

NEXAFS spectroscopy. The spectra were acquired at the C K-edge in the PEY acquisition mode. The retarding voltage was set at −150 V. The primary X-ray beam was linearly polarized with a polarization degree of ~ 90%. The energy resolution was ~ 0.3 eV. The incidence angle of the primary X-rays was varied from 90° with respect to the sample surface (electrical field vector perpendicular to the surface normal) to 20° (electrical field vector nearly parallel to the surface normal) in steps of 10°–20°. In this way, possible linear dichroism in X-ray absorption was monitored, providing information about the orientational order and molecular orientation in the monolayers [28].

The raw spectra were normalized to the incident photon flux by division by a spectrum of a clean, freshly sputtered gold sample [28]. Afterwards, linear pre-edge background was subtracted and the spectra were normalized to the edge jump (determined by a nearly horizontal plateau 40–50 eV above the respective

absorption edges). The energy scale was calibrated to the most intense π* resonance of highly oriented pyrolytic graphite at 285.38 eV [29].

Simulation of the NEXAFS spectra. For the interpretation of the NEXAFS data, the molecular orbitals and the C K-edge NEXAFS spectra of an isolated PFCH molecule with a butyl group as alkyl backbone (PFCH-4) were calculated using the StoBe-deMon package [30]. For geometry optimization and single-point calculations, Becke and Perdew exchange and correlation functionals [31–33] were used. To describe the valence electrons, we employed a double-zeta basis and effective core potentials [34] with a 321/311/1 basis set for hydrogen and carbon, respectively. The core-excited atoms were described using diffuse IGLO-III basis sets [35]. The transition probabilities were calculated by the half core–hole transition potential method [36]. The energies of the transitions were determined using a Δ (Kohn–Sham self-consistent field) approach that includes differential relativistic effects associated with the removal of one electron from the respective 1s orbital [36].

Infrared (IR) spectroscopy. All measurements were carried out using a Thermo Scientific Nicolet 6700 Fourier-transform infrared (FT-IR) spectrometer with a narrow-band mercury-cadmium-telluride semiconductor detector. The optical pathway was continuously purged with dried and CO_2-free air. Bulk substances were characterized using the Smart Performer unit (attenuated total reflection, ATR), while SAMs were analyzed using the Smart SAGA unit with a resolution of 4 cm^{-1} operating with p-polarized light at an angle of incidence of 80° relative to the surface normal. Background spectra of a C12-D SAM on Au(111) were recorded every three measurements except for the exchange experiments in the course of which the spectra were additionally measured against a C16 SAM on Au(111) as background to determine the content of C12-D deposited during the exchange experiment. 256 scans per sample were averaged and the resulting spectra were mildly baseline-corrected. For band assignment, density-functional theory (DFT) calculations were carried out at the BP86 [31, 32] level using the def2-SVP [37] basis set with the ORCA 4.0 [38] program. Molecular geometries were optimized prior to the calculation of IR spectra using the same software package.

Work function. Work function measurements were carried out using a UHV Kelvin Probe 2001 system (KP Technology Ltd., UK). The pressure in the UHV chamber was ~ 10^{-8} mbar. The work function values were referenced to that of a C16 SAM on Au(111), viz. 4.32 eV [39].

Contact angle/wetting properties. After analysis with infrared reflection–absorption (IRRA) spectroscopy, at least two substrates per molecule were measured with a contact angle goniometer (OPTREL) using the static sessile drop method with water as the working fluid. To prevent evaporation during the measurements, the measuring chamber was laid out with wetted cloth 1 h prior to the experiments. For each sample, three different spots were measured.

Exchange experiments. All exchange experiments were carried out with 1 cm × 2 cm substrates prepared as stated previously (see *Monolayer preparation*). The experiments were performed with the primary SAMs of C12, PFCH-11 or PFCH-12 and C12-D as the potential exchange compound. After the deposition of the primary SAMs, their complete characterization by ellipsometry and IRRA spectroscopy was carried out, before the samples were placed in an 0.1 mM exchange solution of C12-D (ethanol, p.a. grade, degassed) for 1, 2, 5 or 20 h, rinsed with ethanol (p.a. grade) after removal from the solution, and blown dry by a stream of nitrogen. Then, characterization with IRRA spectroscopy was performed to determine the changes brought by the exchange reaction. The spectra were measured using both C16 and C12-D SAMs as background and analyzed using the band area tool of the OMNIC software. The obtained band areas for selected IR bands were compared to either the initially measured IRRA spectra before the exchange reaction or to the average band area of the reference, single-component SAMs. For the primary C12, PFCH-11, and PFCH-12 SAMs, the IR bands in the area between 3050 and 2800 cm^{-1} were chosen for the analysis, whereas the bands between and 2050 cm^{-1} were selected to determine the content of perdeuterated molecules in the SAMs. For comparison, the inverse exchange experiments were also performed.

3 Results and discussion

3.1 Synthesis

The target molecules PFCH-11 and PFCH-12 were prepared as illustrated in the synthesis route in Scheme 1, which was basically identical for the odd (C11) and even (C12) thiols. The route used protocols recently reported [17] for the synthesis of long chain fatty acids and alcohols terminated with the same PFCH motif. This involved a Horner–Wardsworth–Emmons olefination of aldehyde I and phosphonate II to generate methyl ester III. A key reaction involved concomitant aryl and vinyl hydrogenation of methyl ester III using Zeng's catalysts and following the protocol developed by Glorius et al. [11], to give the saturated ester IV. Reduction to the alcohol and then mesylation allowed nucleophilic displacement with thioacetate to insert the sulfur atom [40]. Finally, acid hydrolysis released the desired thiols, which were purified by chromatography and made available for surface deposition.

3.2 XPS

Representative XPS spectra of the PFCH-11 and PFCH-12 monolayers are presented in Fig. 2. The S 2p spectra of these films in Fig. 2(a) each exhibit a single S $2p_{3/2,1/2}$ doublet at a BE of ~ 162.0 eV (S $2p_{3/2}$) characteristic of the thiolate–gold bond [41]. This suggests that all molecules in the films are bound to the substrate by the thiolate anchor, corresponding to the typical SAM architecture. No traces of other sulfur-derived species, including physisorbed or oxidized ones, are observed, underlining the chemical homogeneity of the films.

The C 1s spectra of the PFCH-11 and PFCH-12 SAMs in Figs. 2(b) and 2(c) represent a combination of several peaks, as given by the respective fits. The peak at a BE of ~ 284.7 eV (1) stems from the carbon atoms in the alkyl chain, the one at a BE of 287.8–287.9 eV (3) is related to the carbon atoms in the terminal pentafluorocyclohexyl ring of the PFCH-*n* molecules, except for the atom adjacent to the alkyl chain, represented by a peak at 285.5 eV (2). These assignments are supported by the literature data for other fluorine-substituted SAMs [26] as well as by the PE dependence of the relative intensity of the individual peaks in the C 1s spectra. Indeed, the relative intensity of peak 1 increases noticeably as the PE increases from 350 to 580 eV (compare Figs. 2(b) and 2(c)), corresponding to a stronger contribution from a deeper laying part of the monolayers at the higher kinetic energy of the photoelectrons. Note that the attenuation effects, which are particularly strong at the given kinetic energies of the C 1s photoelectrons [42] and the extent of which depends strongly on the exact position of a particular carbon atom in the upright-oriented (see the next section) molecular backbones, modulate strongly the intensities of the individual peaks in the C 1s spectra. Consequently, the intensity relations between these peaks do not reproduce exactly the stochiometric composition of the assembled molecules. Also, because of the particularly strong attenuation, the contribution of the C atom [43] bound to the sulfur atom, cannot be recognized in the spectra.

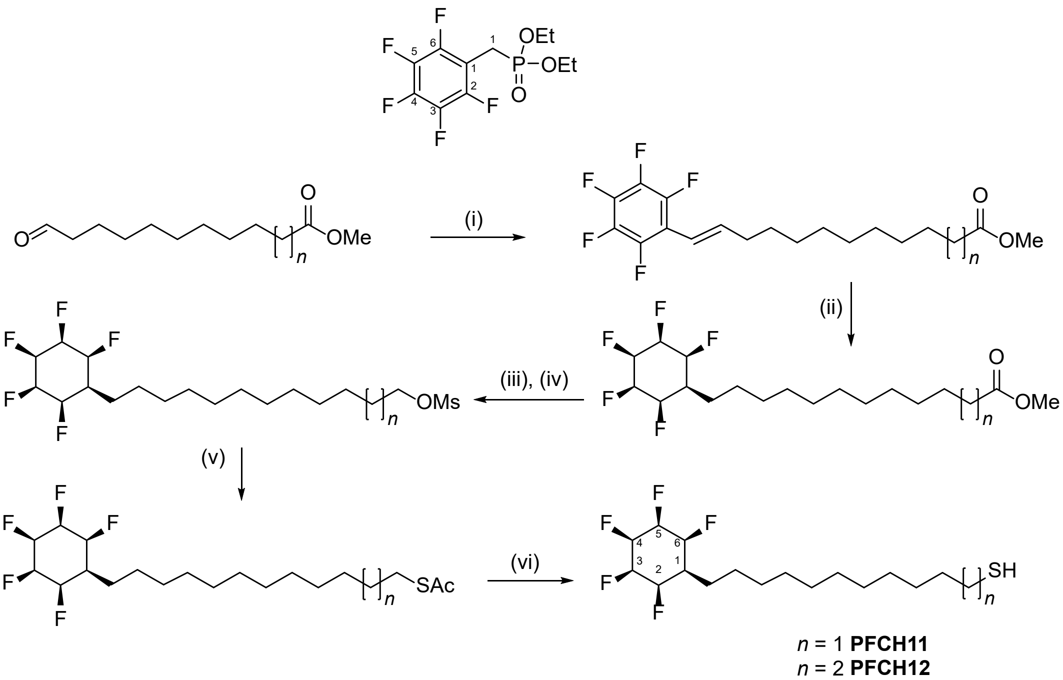

Scheme 1 Synthetic route to PFCH-11 and PFCH-12. Reagents and conditions; (i) NaH, tetrahydrofuran (THF), 50 °C, n = 1: 60%, n = 2: 70%; (ii) H_2, 50 bar, 4 Å molecular sieves, (cycloocta-1,5-dienyl)(2-(2,6-diisopropylphenyl)-3,3-dimethyl-2-azaspiro[4.5]decan-1-yl)rhodium chloride (3 mol%) [11], rt, 24 h, n = 1: 69%, n = 2: 68%; (iii) diisobutylaluminum hydride (DIBAL-H), dichloromethane (DCM), 20 °C, n = 1: 79%, n = 2: 78%; (iv) methanesulfonyl chloride (MsCl), triethylamine (Et_3N), DCM, 0 °C, 2 h, n = 1: 71%, n = 2: 83%; (v) potassium thioacetate (KSAc), DMF, 16 h, n = 1: 84%, n = 2: 87%; (vi) HCl, methanol (MeOH), reflux, 16 h, n = 1: 65%, n =2 : 60%.

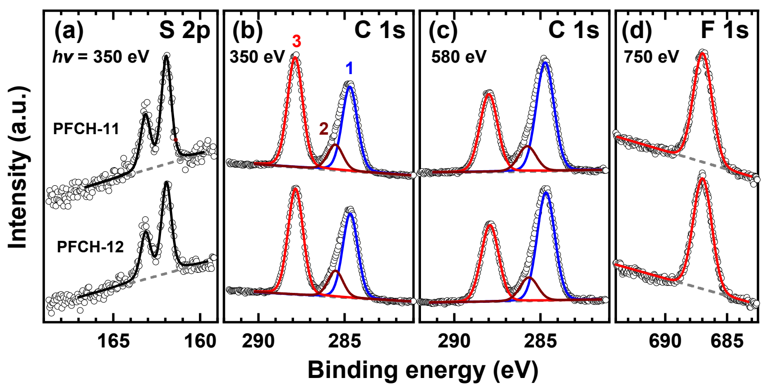

Figure 2 (a) S 2p, (b) and (c) C 1s, and (d) F 1s XP spectra of the PFCH-11 and PFCH-12 SAMs on Au(111). The primary photon energies used to record these spectra are given in the panels. The spectra are fitted by a single doublet (S 2p), a single peak (F 1s), or a combination of several peaks (C 1s) depicted in different colors and marked by numbers; see text for details. Background is drawn by gray dashed lines.

The F 1s spectra of the PFCH-11 and PFCH-12 SAMs in Fig. 2(d) exhibit a single peak at a BE of ~ 687.0 eV, stemming from the fluorine atoms in the pentafluorocyclohexyl ring of the PFCH-*n* molecules. The spectra of the PFCH-11 and PFCH-12 SAMs in Fig. 2 exhibit similar intensities of the characteristic peaks and doublets. Using these intensities, the effective thicknesses and packing densities of these monolayers were calculated and compared to the thicknesses determined from ellipsometry (Table 1). The former parameter was derived based on the Au 4f signal of the substrate, which becomes attenuated by the PFCH-*n* overlayer. Alternatively, the same information can be extracted from the C 1s/Au 4f intensity ratio [44]. The packing densities were evaluated on the basis of the S 2p/Au 4f intensity ratio, assuming similar attenuation of the respective signals. Literature values of the attenuation lengths of the photoemission signals at the relevant kinetic energies were used [45]. The spectrometer-specific coefficients were determined by using a reference C16 SAM with well-known thickness (1.89 ± 0.02 nm) and packing density (4.63×10^{14} molecules/cm^2) [46]. The derived values of the effective thicknesses in Table 1 are in good agreement with the parameters obtained by ellipsometry and are comparable with the molecular lengths (1.98 and 2.05 nm for PFCH-11 and PFCH-12, respectively), once more supporting the monolayer character of the PFCH-*n* films. As expected, the thickness of the PFCH-12 SAM is larger than that of the PFCH-11 monolayer. However, the packing density of the PFCH-12 SAM is slightly lower than that of the PFCH-11 monolayer, which is probably related to the odd-even effects alluded to in Introduction. These effects typically lead to different orientations of the tail group, an important factor for the monolayer packing as well as the surface polarity [47–51]. Apart from this difference, the packing densities of both PFCH-*n* SAMs are noticeably lower than those of non-substituted alkanethiolate monolayers on the same substrate, viz. 4.63×10^{14} molecules/cm^2 [46]. This is, however, understandable, in view of the steric impact of the terminal PFCH group, which dictates the molecular packing rather than the less bulky alkyl chains.

3.3 NEXAFS spectroscopy

The C K-edge NEXAFS spectra of the PFCH-11 and PFCH-12 SAMs and those of the reference C16 monolayer are presented in

Table 1 Effective film thicknesses and packing densities determined by the different approaches. The error for the ellipsometric values was ±0.03 nm, the thickness by XPS ±0.2 nm and the packing density ±10%.

SAM	Thickness (ellipsometry) (nm)	Thickness (from Au 4f) (nm)	Thickness (from C 1s/ Au 4f)(nm)	Packing density (molecules/cm^2)
PFCH-11	1.89	1.93	1.89	3.2×10^{14}
PFCH-12	1.92	1.99	1.92	3.0×10^{14}

Fig. 3. Two types of spectra are shown. The spectra acquired at an X-ray incident angle of 55° ("magic angle") are exclusively representative of the electronic structure of the SAMs and are not affected by orientation effects [28]. In contrast, the 90°–20° difference spectra are representative of the linear dichroism effects, providing information on the orientational order and molecular orientation in the SAMs [28]. The spectra exhibit several pronounced resonances, viz. those at ~ 285.1 eV (1), 287.2–287.8 eV (2), ~ 289.4 (3), 291.1 (4), ~ 294.8 (5), and ~ 301 eV (6). Resonance 1, being comparably weak and revealing no dichroism, is most likely related to a minor contamination (C=C), which might have been induced by the interaction with the photoelectrons [28]. Feature 2, observed both for the PFCH-*n* SAMs and the reference C16 monolayer and exhibiting a pronounced linear dichroism, represents the so-called 'C–H' band of the alkyl chains and is comprised of several σ^*_{C-H}/R resonances [52–58]. Resonances 3 and 4, not observed for the C16 SAM and exhibiting pronounced linear dichroism, stem most likely from the terminal PFCH group of the PFCH-*n* molecules. Resonances 5 and 6, observed for both PFCH-*n* and C16 SAMs, exhibit a linear dichroism, which presumably represents transitions into σ* C–C orbitals of the alkyl backbone and the PFCH moiety.

For the following discussion, the directions in the molecules are visualized in Fig. 4, along with the lowest occupied molecular orbital (LUMO) calculated using ORCA 4.0, BP-86 functional, and def2-SVP as basis set. As it can be seen, the LUMO is arranged basically coplanar to the ring plane spanned by vectors **B** and **C**.

To support the tentative assignments of resonances 3 and 4, important for the further analysis, we have performed DFT calculations of the NEXAFS spectra of the PFCH-n molecules using a butyl group instead of the longer ω-mercaptoalkyl groups (PFCH-4). The details can be found in Figs. S1 and S2 and the related discussion in the Electronic Supplementary Material (ESM). The calculated NEXAFS spectra of the PFCH ring of PFCH-4 are shown in Fig. 5 for the anisotropic case (without polarization) as well as for the orientations of the electric field vector perpendicular (**A**) and parallel to the ring plane (**B** and **C**). These spectra exhibit several characteristic absorption resonances and pronounced linear dichroism, as additionally emphasized by the difference spectrum. The spectrum of the PFCH ring is dominated by the pronounced resonance at ~ 290.6 eV accompanied by a weaker resonance at ~ 291.6 eV. These resonances, representing the transitions into the LUMO and LUMO+1 orbitals of PFCH, correspond to the resonances 3 and 4 in the spectra of the PFCH-*n* SAMs in Fig. 3. The slight energy difference (~ 1.2 eV) is related to the limited accuracy of DFT calculations in this regard, but the pattern of these resonances mimics well the experimental data, especially in the difference spectra.

The molecular orbitals related to the 'C–H' band build a plane orbital, which is perpendicular to the main axis of the alkyl backbone, while the LUMO orbital of the PFCH ring is better described as a vector orbital, with contributions provided by individual C–F bonds. The well-defined orientation of these

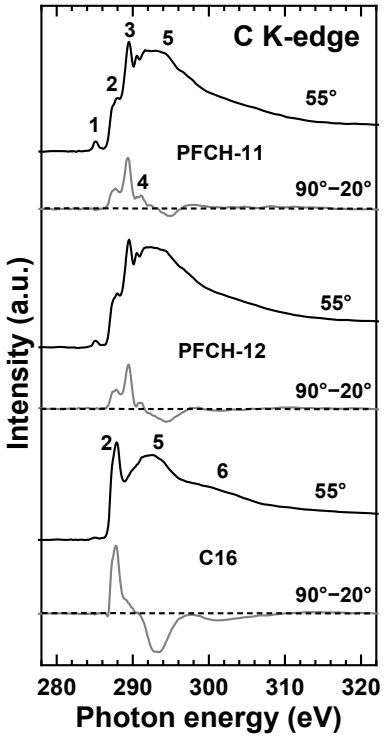

Figure 3 C K-edge NEXAFS spectra of the PFCH-11 and PFCH-12 SAMs on Au(111), along with the data for the reference C16 monolayer. The spectra acquired at an X-ray incident angle of 55° (black curves) and the difference between the spectra acquired at X-ray incident angles of 90° and 20° (gray curves) are presented. The most important absorption resonances are marked by numbers (see text for details). Horizontal dashed lines correspond to zero.

orbitals with respect to the molecular framework allows the molecular orientation of the SAMs to be determined. For this purpose, we applied the standard theoretical framework for the plane and vector molecular orbitals [28]. Within the respective evaluation procedure (Fig. 6), the intensities of the 'C–H' and C*–F resonances I were derived from the experimental spectra, plotted as a function of the X-ray incidence angle θ and fitted by the suitable theoretical curves for the plane case

$$I(\gamma,\theta) = AP\cdot 2/3[1-1/4(3\cos^2\theta-1)(3\cos^2\gamma-1)] + (1-P)\cdot 1/2[1+\cos^2\gamma] \quad (1)$$

and the vector case

$$I(\alpha,\theta) = BP1/3[11/2(3\cos^2\theta-1)(3\cos^2\alpha-1)] + (1-P)1/2\sin^2\alpha \quad (2)$$

where A and B—constants, P—the polarization degree of the primary X-rays, γ—the average angle between the normal of the plane orbital and surface normal, and α—the average tilt angle of the vector orbital with respect to the surface normal [28].

To derive the resonance intensities, the spectra were decomposed to a superposition of two absorption edges, corresponding to the C–C/C–H and C–F moieties, respectively, and a variety of absorption resonances. An example is shown in Fig. 6(a); the full set of the decomposition data is presented in Figs. S3 and S4 in the ESM). The derived angular dependence of the 'C–H' and C*–F resonance intensities is presented in Figs. 6(b) and 6(c), respectively, along with corresponding fits performed according to Eqs. (1) and (2) [28]. Note that for simplicity, we did not use the absolute intensities but the intensity ratios, following an established procedure [59]. Note also that whereas only the fits for the $I(\theta)/I(55°)$ ratio are shown in Figs. 6(b) and 6(c), the analogous fits were also performed for the $I(\theta)/I(20°)$, $I(\theta)/I(30°)$, and $I(\theta)/I(90°)$ (see Figs. S5 and S6 in the ESM), and the average

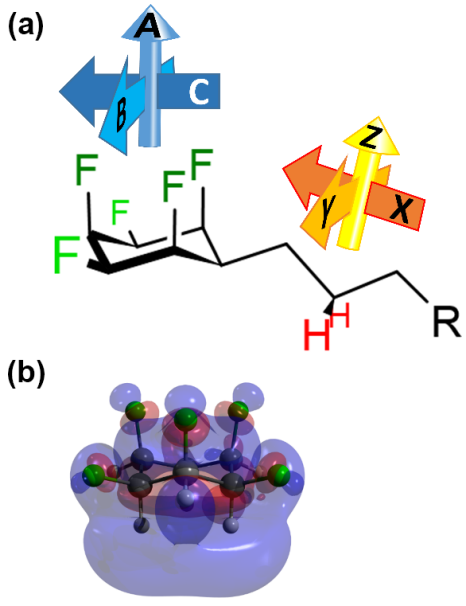

Figure 4 (a) Directions in the PFCH molecules. The molecular 'plane' of the cyclohexane ring is defined by the vectors A, B, and C, with A being parallel to the axial C–F bonds (dark green F atoms). The coordinate system of the alkyl chain is independent and defined by the CH_2 planes, which are spanned by the vectors Y and Z. Vector X basically describes the orientation of the alkyl chain axis in the all-*trans* conformation. (b) The LUMO of PFCH-11 (seen along the long axis of the molecules). The nodal planes are parallel to the ring plane, so the respective orbital vector is parallel to direction A.

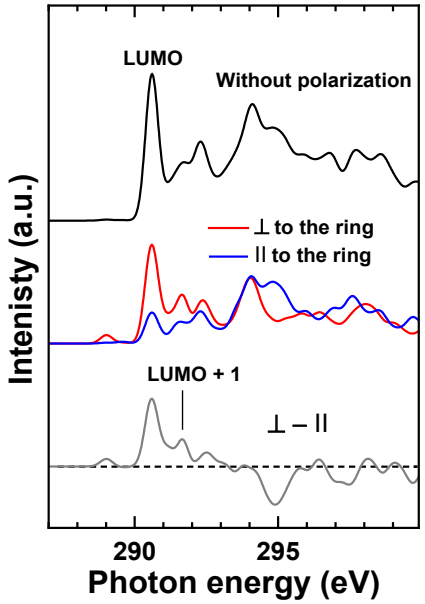

Figure 5 Calculated C K-edge NEXAFS spectra of the PFCH moiety of PFCH-4 without polarization (black curve) and for two different orientations of the electrical field vector with respect to this moiety (red and blue curves) along with the respective difference spectrum (gray curve). Absorption resonances corresponding to the LUMO and LUMO+1 orbitals are marked. The horizontal dashed line corresponds to zero.

over the tilt angles derived from the four was calculated. The resulting values of the average tilt angles are compiled in Table 2. Note that γ, which is parallel to the vector **X** in Fig. 4, corresponds directly to the average tilt angle of the alkyl backbone with regard to the surface normal, while the average tilt angle of the PFCH 'plane' is given by 90° – α (with α being parallel to **A**). Consequently, the PFCH moieties are less tilted than the respective alkyl linkers, driven most likely by the tendency to achieve the maximal possible packing density at the given molecular conformation. As to the alkyl linkers, the respective

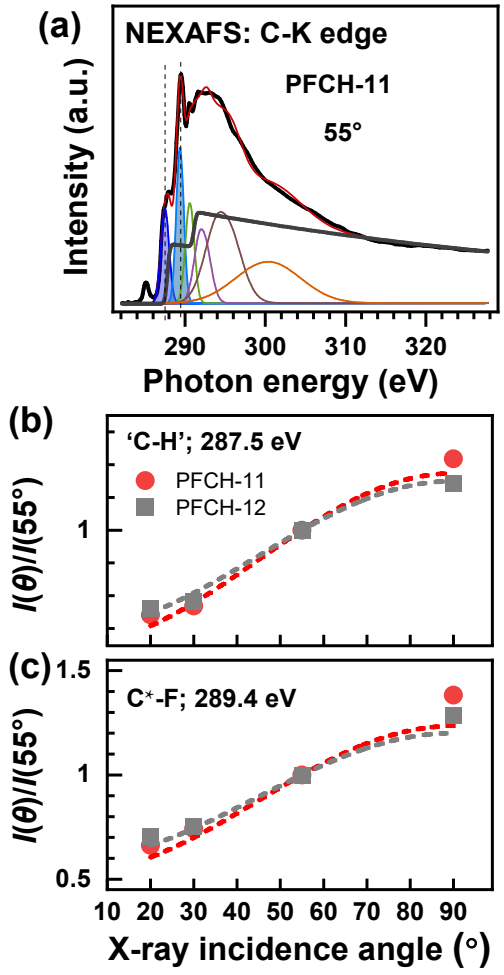

Figure 6 (a) Decomposition of a representative NEXAFS spectrum of the PFCH-*n* SAMs; the most relevant 'C–H' and C*–F resonances are shadowed in violet and blue, respectively. (b) and (c) The angular dependence of the (b) 'C–H' and (c) C*–F resonance intensity ratio $I(\theta)/I(55°)$ for the PFCH-11 (red circles) and PFCH-12 (gray squares) SAMs, along with the respective fits, according to Eqs. (1) and (2) (color-coded dashed lines).

average tilt angles (39° and 41.5°) are noticeably larger than those of the well-ordered, non-substituted alkanethiolate SAMs on Au(111), such as C16 (~ 33°) [60, 61]. This is understandable in view of significant disturbance of the alkyl matrix by the presence of the bulky PFCH moieties.

It is interesting that the derived average tilt angles in the PFCH-11 SAM are lower than the ones in the PFCH-12 monolayer. This behavior correlates well with the difference in the packing density between these SAMs (see Section 3.2) and is most likely related to odd-even effects, discussed shortly in Section 3.2. Significantly, the differences between the average molecular tilt angles in the PFCH-11 and PFCH-12 SAMs could be additionally verified by the difference spectra approach; the respective data and discussion can be found in Fig. S7 and the related discussion in the ESM.

3.4 IR spectroscopy

IR spectroscopy is not only a very versatile technique to identify chemical groups, but in conjunction with metal surfaces also permits the determination of the orientation of these groups with respect to the substrate [62, 63]. For assignment of specific vibrations and the orientation of the respective transition dipole moments (TDMs), the IR spectra of the bulk precursor materials were measured using an ATR setup and compared to the spectra calculated by DFT as well as the SAM spectra. Designated ranges of the IRRA (SAM), ATR (bulk) and calculated (DFT) spectra for PFCH-11 and PFCH-12 are compared in Fig. 7 (the full range

Table 2 Average tilt angles of the 'C–H' and C*–F orbitals and the respective average tilt angles of the PFCH moieties in the PFCH-*n* SAMs. All angles are defined with respect to the surface normal. The accuracy of the values is ±3°.

SAM	Tilt angle γ of 'C–H' orbital	Tilt angle α of C*–F orbital	Tilt angle of PFCH plane
PFCH-11	39°	67°	23°
PFCH-12	41.5°	65°	25°

spectra and band assignments can be found in Figs. S8 and S9 and Tables S1 and S2 in the ESM). Not surprisingly, the bulk spectra of PFCH-11 and PFCH-12 are similar to each other and are well described by the calculated spectra. Analysis of the C–H stretching vibrations in the spectra of both SAMs reveals mostly all-*trans* conformation of the alkyl backbones, with the position of the asymmetric CH_2 stretching vibration of the alkyl chains (2920 cm^{-1}) indicating the presence of only few *gauche* defects as compared to non-substituted alkanethiolate SAMs [64, 65]. These defects are presumably caused by the steric demand of the bulky PFCH groups leading to some reorientations in the upper alkyl chain segments to permit optimal arrangement of the PFCH groups.

The spectra illustrated in Fig. 7 indicate that the intensities of several bands are diminished in the spectra of the SAMs compared to the ones of the bulk materials. This can be attributed to surface selection rules on metal surfaces, where the intensities of vibrations with TDM parallel to the surface are extinguished, while signals with TDM perpendicular to the surface, therefore parallel to the surface normal, become enhanced. The analysis of the relative change of the signal intensities allows calculation of the orientation of individual groups in the SAMs [62, 63]. For the following discussion, we will use the same directions as shown in Fig. 4.

For PFCH-11, the major C–F stretching vibrations with a TDM along the **A** axis at 1158 cm^{-1} (axial, in-phase), 1129 cm^{-1} (axial, anti-phase) and 1070 cm^{-1} (equatorial, symmetric) are clearly attenuated in the IRRA spectrum compared to ATR, indicating that the **A** axis of the adsorbed molecules is oriented almost parallel to the surface. This is also supported by the C–C vibration of the ring at 940 cm^{-1} and the C–F vibration of the axial F atoms at 796 cm^{-1}, which are significantly reduced in the IRRA spectra and exhibit TDMs in the **A** direction as well. In contrast, the vibrations at 1050, 867 and 778 cm^{-1} with TDMs in the **B** and **C** directions are not weakened significantly. This can only occur if the **B** and **C** axes of the adsorbed molecules are canted about 45° towards the surface indicating a tipping of the ring within the ring plane, which also has been observed in X-ray structures of long chain PFCH derivatives [17]. Lastly, the vibration of the alkyl chain at 725 cm^{-1} is extinguished, while the vibration at 715 cm^{-1} is still present in the IRRA spectrum. These vibrations show TDMs along the **Y** and **Z** axis, respectively, indicating that the chain is tilted in one direction and not twisted, further supporting the hypothesis of an alkyl chain mostly in the all-*trans* conformation.

Analysis of the IR data for the PFCH-12 SAM (see Fig. 7, right panel) gives similar results with slightly more tilted PFCH tail groups. As the odd-even effects typically cause a significant reorientation of the tail groups, this must go together with some *gauche* defects, presumably in the upper part of the alkyl chains, as the IR spectra indicate a mostly all-*trans* conformation. Generally, both ATR (bulk) and IRRA (SAM) spectra of PFCH-12 are very similar to those of PFCH-11, indicating similar structures for both PFCH-11 and PFCH-12 SAMs, which is in good agreement with the NEXAFS results.

3.5 Wetting properties

Typically, highly fluorinated surfaces have a very low surface energy, which results in a very limited wettability, often with water contact angles (WCAs) well above 100° [66]. Surprisingly, the WCAs of the PFCH-*n* monolayers (Table 3; along with some reference values) are lower at ~ 63°.

The WCAs of both PFCH-*n* SAMs are identical and in line with the similarities of their tail-group orientations. Apart from this, the WCAs are significantly lower than those reported for non-substituted alkanethiols (here, a C12-D SAM was used as a reference with a WCA of 113°) and for perfluoroalkyl-terminated thiols. Several possibilities exist to explain this observation. First, the layers are not well-ordered. This can, however, be excluded by the XPS, NEXAFS and IR data, which all suggest densely packed and highly ordered monolayers. Second, the SAM–ambient interface is not comprised of well-oriented CH_3 or CF_3 groups presenting a predominantly hydrocarbon or fluorocarbon moiety, but rather the ring edges of the PFCH rings are presented at the surface. Nevertheless, this apparently does not lead inherently to

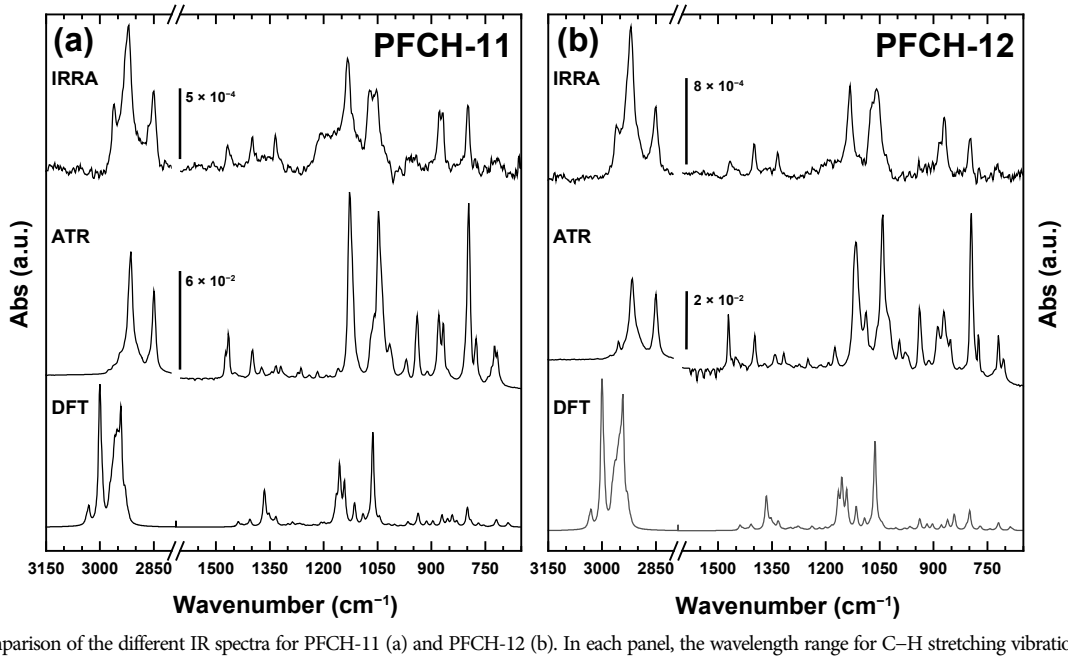

Figure 7 Comparison of the different IR spectra for PFCH-11 (a) and PFCH-12 (b). In each panel, the wavelength range for C–H stretching vibrations is on the left side, while the fingerprint range is on the right.

reduced contact angles, as it has been reported that cyclohexyl alkanthiolate SAMs and undecafluorocyclohexyl alkanethiolate SAMs show WCAs of 107° and 119°, respectively [67]. Also, the WCA of the phenyl-terminated biphenylthiolate SAM on Au(111), containing no fluorine at all, is higher than the PFCH-*n* values in Table 3 [68, 69] Third, the rings expose fluorine as well as hydrogen atoms, leading to some kind of micro heterogeneity. Surprisingly, SAMs consisting of mixtures of the cyclohexyl thiolate and perfluorocyclohexyl thiolate do not show decreased WCA but rather a continuous variation of the WCA depending on the SAM composition [70].

This suggests that the very high dipole moment **parallel** to the surface must induce the significantly lowered WCAs. Apparently, the dipoles near the surface result in an enhanced interaction with the water molecules (presumably by reorientation), increasing thus the wetting. This is consistent with the significant lowering in log*P* values when comparing derivatives of PFCHs with the corresponding cyclohexyl derivatives and suggests that the polarized hydrogen atoms ($H^{\delta+}$-C-$F^{\delta-}$) make hydrogen bonding contact with water molecules [71].

3.6 Work function

The work function is an additional descriptor for SAMs, which is determined by the packing density, the molecular orientation as well as conformation. The SAM-induced change in the work function $\Delta\Phi$ is generally described by the equation

$$\Delta\Phi = \rho_{SAM} \times (\mu \times \cos\beta/\varepsilon_0\varepsilon_{SAM} + \mu_{binding}/\varepsilon_0\varepsilon_{binding}) \quad (3)$$

where ρ_{SAM} is the molecular packing density, μ the dipole moment of the dipolar group, β the tilt angle of the dipolar group, ε_{SAM} dielectric constant of the SAM, ε_0 the vacuum permittivity, $\mu_{binding}$ contribution to the dipole associated with the binding of the SAM to the substrate, and $\varepsilon_{binding}$ the respective dielectric constant [72].

The work functions of the PFCH-11 and PFCH-12 SAMs are shown in Fig. 8, along with the reference value for the non-substituted C16 monolayer. The latter value represents the effect of the binding dipole with respect to the work function of clean gold, the latter being 5.33 eV for single crystalline Au(111) surfaces [73] and 5.1–5.2 eV for clean, evaporated Au films with (111) texture [74]. As expected, the decoration of the alkanethiolate backbones with the electronegative PFCH groups results in an increase of the work function. Nevertheless, this increase (by 0.5–0.7 eV) is rather moderate compared to other SAMs with fluorinated tail groups or partly fluorinated molecular chains, which typically end up at 5.5–5.96 eV (increase by 1.2–1.6 eV) [22, 75–77]. This difference can be at least partly understood by the lower packing densities of the PFCH-*n* films compared to the C16 SAM (see Table 1) but it would be not enough.

This behavior can be explained by the orientation of the dipolar elements within the SAM. As stated before, the Janus motif of the PFCH rings results in an extraordinarily high dipole moment, which, if oriented completely perpendicular to the surface with the fluorine atoms up, would presumably result in work functions well above 6 eV. With the tilt angles determined in Section 3.3 (α = 23° and 25°), this contribution should be much smaller ($\cos\beta \approx 0.4$; the dipole moment is nearly perpendicular to the PFCH plane), explaining the much smaller work functions. Interestingly, the determined values for both kinds of SAMs permit a distinction of the orientation of the Janus faces of the PFCH moieties. While NEXAFS and IRRA spectroscopy allow for the determination of the orientation of the vectors with respect to the surface normal, they cannot distinguish between the algebraic signs of the vectors. This is not of importance for highly symmetric moieties, such as phenyl rings or longer alkyl chains, but makes a big difference in case of the PFCH unit with the majority of its dipole moment being oriented antiparallel to the vector **A** drawn in Fig. 4. In fact, if the ring were to be flipped over such that the axial hydrogen atoms were directed towards the SAM surface, the work function should become significantly reduced, possibly even below that of the C16 SAMs. To the best of our knowledge, only a couple of systems are known, in which hydrogen atoms are exposed at the SAM–ambient interface with fluorine atoms 'buried' below them [78] and unfortunately no work functions were reported for these monolayers yet.

Table 3 WCA measured by the static sessile drop method. Reference images of the droplets are provided in Fig. S10 in the ESM.

	Blank Au	C12-D	PFCH-11	PFCH-12
Contact angle	30° ± 3°	113° ± 2°	63° ± 1°	63° ± 1°

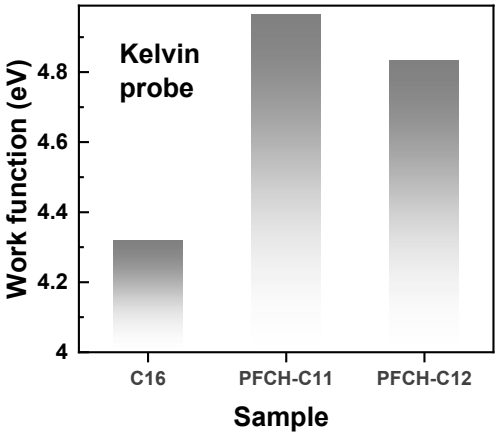

Figure 8 Work functions of the PFCH-11 and PFCH-12 SAMs on Au(111), along with the value for the reference C16 monolayer. The accuracy of the values is ±0.05 eV.

Although the odd-even effects in this system are small, they are clearly revealed in the work function data as well as in the orientation data. With a higher tilt angle of the PFCH plane in the PFCH-12 SAM, an increased work function would result if the 'fluorine face' would be oriented towards the SAM surface (= away from the Au surface). As the contrary is the case, it can be assumed that the hydrogen atoms are directed upwards. It is worth mentioning that this is consistent with the conformation of the PFCH-alkyl system found in the X-ray structure of PFCH-13-OH [17], as this permits an optimal interlocking of the PFCH units by head-to-tail stacking (promoted by the intermolecular H···F bonds) [17, 79], while also accommodating the alkyl chains in the all-*trans* conformation with maximized van-der-Waals interactions.

3.7 Exchange experiments

The head-to-tail arrangement of the PFCH units typically results in crystals with a high melting point, indicative for strong intermolecular interactions [17]. It is of interest to explore if this arrangement, which is apparently also present in these SAMs, leads to an increased layer stability when compared, e.g., to non-substituted alkanethiolate SAMs. Therefore, exchange experiments were carried out, in which the monolayers of PFCH-11, PFCH-12 and of C12 (as a reference) were immersed in solutions of C12-D for different time periods. The composition of the SAMs after the exchange reaction was determined by IRRAS as the signals of the components were distinct and allowed for reliable integration. The results obtained are shown in Fig. 9, with a full set of data as well as the fit parameters available in Table S3 and Figs. S11–S13 in the ESM).

The general behavior of all three SAMs is similar in the exchange experiments. After an initial phase of rapid changes to

the SAM composition, the systems level off reaching a composition with a remaining content of the starting material between 70% and 80%, while the accompanying growth in the C12-D content stagnates around 21% for all systems tested. Therefore, a one-to-one exchange of the SAM-forming molecules is proposed, although the PFCH-*n* molecules have higher steric demand than the C12-D and no complete exchange of the primary monolayer is observed. This behavior is known in the literature [80] and indicates an intrinsic kinetic stability of the primary SAM, as the SAM precursors used for the exchange experiments are not able to completely exchange the primary molecules. Although the resulting compositions of the investigated SAMs after 20 h were similar, the exchange of C12 by C12-D proceeds a lot faster than the exchange of PFCH-11 or PFCH-12 by C12-D as quantitatively emphasized by the time constants of the decay functions. The respective time constants for the exchange reactions were determined as 0.9 ± 0.2, 6 ± 3 and 10 ± 6 h, respectively. Thus, the exchange reaction of the PFCH-11 proceeds roughly six times slower and the one of PFCH-12 about ten times slower than the exchange of C12. Thus, the PFCH motif clearly provides an increased kinetic stability for the PFCH-11 and PFCH-12 SAMs, although these layers are significantly less densely packed than the alkanethiole ones. Note that, according to Fig. 9(a), the final resistance of the PFCH-11 SAM to exchange is somewhat higher than that of the PFCH-12 monolayer. This can be explained by the higher packing density of the former SAM (odd-even effects; see Section 3.2) hindering the exchange reaction to some extent.

For the inverse exchange reaction starting with C12-D SAM and using PFCH-*n* as exchange reagents (see Table S3 and Figs. S14–S16 in the ESM) the remaining content of the starting SAM is lowered to 56% (PFCH-11) and 57% (PFCH-12), respectively, while the content of exchange reagent, here PFCH-*n*, in the layer reaches about 30%. This is interesting as now the higher steric demand and therefore the lower packing densities of the PFCH-*n* SAMs influence the exchange ratio, which in this case is about 1.5 to 1, identical to the ratio between the packing densities of non-substituted alkanethiolate SAMs vs. PFCH-*n* monolayers.

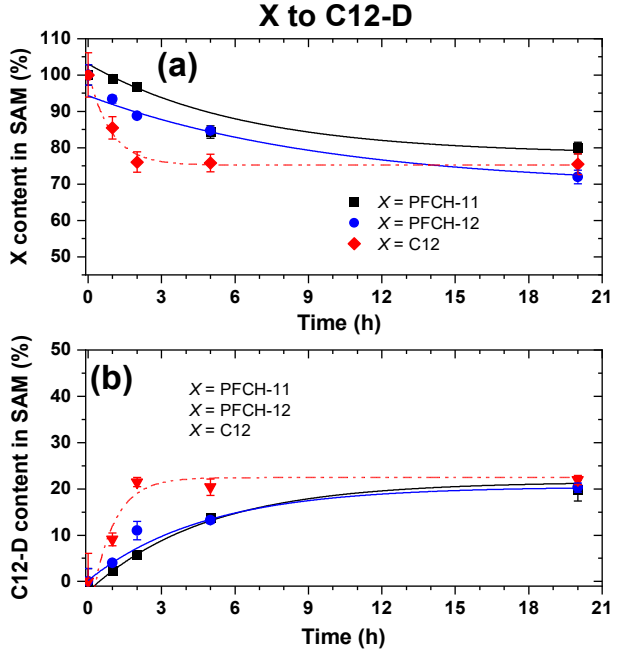

Figure 9 Changes in SAM composition in the course of the exchange experiments, starting with the single-component SAM of molecule X exchanging with C12-D. (a) Remaining content of molecule X in the SAMs. (b) Content of C12-D in the SAMs observed after exchange.

4 Conclusions

In this project, the Janus-faced PFCH motif was successfully implemented in SAMs. Two thiol derivatives with different alkyl chain lengths were synthesized. These molecules form monolayers with thicknesses of about the molecular lengths, suggesting an upright orientation in both kinds of SAMs. The combination of XPS, NEXAFS spectroscopy and IR spectroscopy confirmed this assumption and provided detailed insight into the orientation of the two main parts of the molecular backbone, viz. the PFCH groups and the alkyl chains. For the assignment of individual contributions in the NEXAFS and IR spectra, DFT calculations were performed, which also permitted a determination of the TDMs of the respective transitions. We found that the alkyl chains adopt an almost perfect all-*trans* conformation with an average tilt angle of ~ 40° with respect to the surface normal.

The PFCH groups in both SAMs have similar orientations despite the different numbers of methylene groups in the alkyl chains, which normally leads to pronounced odd-even effects, except when the head groups can be flexibly rotated [81]. It is possible that this kind of adaption also takes place to some extent in the current system, as the PFCH groups in both monolayers are significantly canted within the ring planes, presumably to maximize the intermolecular ring interactions parallel to the surface (dipolar interactions and H···F bridges, Fig. 10). Consequently, the odd-even effects are noticeably reduced in the PFCH-n SAMs, but are still well perceptible in the packing density, molecular orientation, and the stability against exchange, with the right relation to the parity of the methylene group number in the alkyl linker (see Refs. [45–49]). In contrast, these effects are fully compensated in the wetting behavior, which is basically the same for both layers. Surprisingly, the WCAs are much smaller than those of non-fluorinated or perfluoroalkylated alkanethiolate monolayers, even with the cyclohexyl motif [67, 70]. We have to assume that the very strong dipole moment, which is mostly directed parallel to the surface, and the polarizing effect of the fluorine atoms on the geminal hydrogen atoms around the PFCH ring results in strong interactions with the dipolar water molecules, most probably through $H_2O^{\cdots\delta+}H–C–F^{\delta-}$ interactions, consistent also with log*P* reductions in other studies [71]. The remaining surface component of this large dipole moment could be determined by work function measurements. The analysis of the respective data leads us to the conclusion that the axial H atoms point towards the SAM surface. The deduced molecular conformation is similar to the one in the crystal structure of PFCH-13-OH [17], in which both, the dipolar head-to-tail intermolecular ring interaction and the van-der-Waals interaction of the alkyl chains, are maximized. These interactions lead to an increased kinetic stability of the PFCH-*n* SAMs as demonstrated by dedicated exchange experiments performed, in which a part of the PFCH-*n* molecules become replaced by alkanethiols. This is all the more remarkable, as the increased steric bulk of the PFCH tail groups leads to a significantly lowered packing density (3×10^{14} vs. 4.6×10^{14} molecules/cm^2 in non-substituted alkanethiolate SAMs), which normally results in reduced stability against molecular exchange.

The introduction of the PFCH group can thus be considered as a stabilizing motif, which might be useful for improving the properties of SAMs, an issue of general importance. The decoupling of the electrostatic and wetting properties, occurring in the PFCH-n SAMs, can be of interest in the context of organic electronics allowing independent tuning of energy level alignment and chemistry at the interfaces. Along this line, more work should be invested in understanding the influence of the dipole moments parallel to the surface, in particular—in the context of molecular

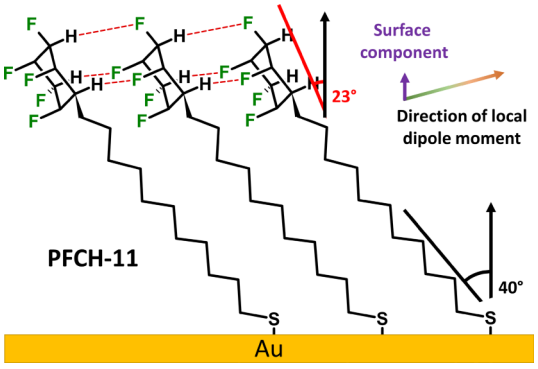

Figure 10 Surface structure of the PFCH-11 SAM as deduced from XPS, NEXAFS spectroscopy, IR spectroscopy, and work function measurements, with intermolecular H–F bonds highlighted as red dashed lines. The conformation is similar to that found in a crystal structure of PFCH-13-OH [17].

electronics, as this represents a new motif compared to other systems with very similar structures. Possible candidates could be p-oligophenyls with strong dipole moments perpendicular to the molecular axis or all-*syn* configured, semifluorinated alkane derivatives ($(CHF)_n$).

Acknowledgments

C. F. and A. T. thank the Fonds der Chemischen Industrie (FCI) for providing a PhD stipend. S. D., Y. B. L. and M. Z. thank the Helmholtz Zentrum Berlin for the allocation of synchrotron radiation beamtime at BESSY II and financial support. Y. L. thanks the China Scholarship Council (CSC) for financial support.

Funding note: Open Access funding enabled and organized by Project DEAL.

Electronic Supplementary Material: Supplementary material (description of the synthesis procedure, nuclear magnetic resonance (NMR) spectra, additional NEXAFS spectroscopy data, full analysis of the IR data, additional contact angle goniometry data, and additional data of the exchange experiments) is available in the online version of this article at https://doi.org/10.1007/s12274-023-5818-4.

References

[1] Kirsch, P. *Modern Fluoroorganic Chemistry*: *Synthesis*, *Reactivity*, *Applications*; 2nd ed. Wiley-VCH: Weinheim, 2013.

[2] Fier, P. S.; Hartwig, J. F. Selective C-H fluorination of pyridines and diazines inspired by a classic amination reaction. *Science* **2013**, *342*, 956–960.

[3] Müller, K.; Faeh, C.; Diederich, F. Fluorine in pharmaceuticals: Looking beyond intuition. *Science* **2007**, *317*, 1881–1886.

[4] Sandford, G. Elemental fluorine in organic chemistry (1997–2006). *J. Fluorine Chem.* **2007**, *128*, 90–104.

[5] Dawood, K. M. Electrolytic fluorination of organic compounds. *Tetrahedron* **2004**, *60*, 1435–1451.

[6] Zhu, W. W.; Zhen, X.; Wu, J. Y.; Cheng, Y. P.; An, J. K.; Ma, X. Y.; Liu, J. K.; Qin, Y. J.; Zhu, H.; Xue, J. J. et al. Catalytic asymmetric nucleophilic fluorination using $BF_3{\cdot}Et_2O$ as fluorine source and activating reagent. *Nat. Commun.* **2021**, *12*, 3957.

[7] Scheidt, F.; Schäfer, M.; Sarie, J. C.; Daniliuc, C. G.; Molloy, J. J.; Gilmour, R. Enantioselective, catalytic vicinal difluorination of alkenes. *Angew. Chem., Int. Ed.* **2018**, *57*, 16431–16435.

[8] O'Hagan, D. Understanding organofluorine chemistry. An introduction to the C–F bond. *Chem. Soc. Rev.* **2008**, *37*, 308–319.

[9] Biffinger, J. C.; Kim, H. W.; DiMagno, S. G. The polar hydrophobicity of fluorinated compounds. *ChemBioChem* **2004**, *5*, 622–627.

[10] Keddie, N. S.; Slawin, A. M. Z.; Lebl, T.; Philp, D.; O'Hagan, D. All-*cis* 1,2,3,4,5,6-hexafluorocyclohexane is a facially polarized cyclohexane. *Nat. Chem.* **2015**, *7*, 483–488.

[11] Wiesenfeldt, M. P.; Nairoukh, Z.; Li, W.; Glorius, F. Hydrogenation of fluoroarenes: Direct access to all-*cis*-(multi)fluorinated cycloalkanes. *Science* **2017**, *357*, 908–912.

[12] Wei, Y.; Rao, B.; Cong, X. F.; Zeng, X. M. Highly selective hydrogenation of aromatic ketones and phenols enabled by cyclic (amino)(alkyl)carbene rhodium complexes. *J. Am. Chem. Soc.* **2015**, *137*, 9250–9253.

[13] Shyshov, O.; Siewerth, K. A.; von Delius, M. Evidence for anion-binding of all-*cis* hexafluorocyclohexane in solution and solid state. *Chem. Commun.* **2018**, *54*, 4353–4355.

[14] Shyshov, O.; Haridas, S. V.; Pesce, L.; Qi, H. Y.; Gardin, A.; Bochicchio, D.; Kaiser, U.; Pavan, G. M.; von Delius, M. Living supramolecular polymerization of fluorinated cyclohexanes. *Nat. Commun.* **2021**, *12*, 3134.

[15] Clark, J. L.; Neyyappadath, R. M.; Yu, C. H.; Slawin, A. M. Z.; Cordes, D. B.; O'Hagan, D. Janus all-*cis* 2,3,4,5,6-pentafluoro-cyclohexyl building blocks applied to medicinal chemistry and bioactives discovery chemistry. *Chem. -Eur. J.* **2021**, *27*, 16000–16005.

[16] Wang, Y.; Lee, W.; Chen, Y. C.; Zhou, Y. H.; Plise, E.; Migliozzi, M.; Crawford, J. J. Turning the other cheek: Influence of the *cis*-tetrafluorocyclohexyl motif on physicochemical and metabolic properties. *ACS Med. Chem. Lett.* **2022**, *13*, 1517–1523.

[17] Clark, J. L.; Taylor, A.; Geddis, A.; Neyyappadath, R. M.; Piscelli, B. A.; Yu, C. H.; Cordes, D. B.; Slawin, A. M. Z.; Cormanich, R. A.; Guldin, S. et al. Supramolecular packing of alkyl substituted Janus face all-*cis*-2,3,4,5,6-pentafluorocyclohexyl motifs. *Chem. Sci.* **2021**, *12*, 9712–9719.

[18] Poskin, T. J.; Piscelli, B. A.; Yoshida, K.; Cordes, D. B.; Slawin, A. M. Z.; Cormanich, R. A.; Yamada, S.; O'Hagan, D. Janus faced fluorocyclohexanes for supramolecular assembly: Synthesis and solid state structures of equatorial mono-, di- and tri-alkylated cyclohexanes and with tri-axial C–F bonds to impart polarity. *Chem. Commun.* **2022**, *58*, 7968–7971.

[19] MacLeod, B. A.; Horwitz, N. E.; Ratcliff, E. L.; Jenkins, J. L.; Armstrong, N. R.; Giordano, A. J.; Hotchkiss, P. J.; Marder, S. R.; Campbell, C. T.; Ginger, D. S. Built-in potential in conjugated polymer diodes with changing anode work function: Interfacial states and deviation from the Schottky-Mott limit. *J. Phys. Chem. Lett.* **2012**, *3*, 1202–1207.

[20] Zojer, E.; Terfort, A.; Zharnikov, M. Concept of embedded dipoles as a versatile tool for surface engineering. *Acc. Chem. Res.* **2022**, *55*, 1857–1867.

[21] Liu, Y. B.; Katzbach, S.; Asyuda, A.; Das, S.; Terfort, A.; Zharnikov, M. Effect of substitution on the charge transport properties of oligophenylenethiolate self-assembled monolayers. *Phys. Chem. Chem. Phys.* **2022**, *24*, 27693–27704.

[22] Liu, Y. B.; Zeplichal, M.; Katzbach, S.; Wiesner, A.; Das, S.; Terfort, A.; Zharnikov, M. Aromatic self-assembled monolayers with pentafluoro-λ⁶-sulfanyl ($-SF_5$) termination: Molecular organization and charge transport properties. *Nano Res.*, in press, https://doi.org/10.1007/s12274-022-5350-8.

[23] Raiber, K.; Terfort, A.; Benndorf, C.; Krings, N.; Strehblow, H. H. Removal of self-assembled monolayers of alkanethiolates on gold by plasma cleaning. *Surf. Sci.* **2005**, *595*, 56–63.

[24] Nefedov, A.; Wöll, C. Advanced applications of NEXAFS spectroscopy for functionalized surfaces. In *Surface Science Techniques*. Bracco, G.; Holst, B., Eds.; Springer: Berlin, 2013; pp 277–303.

[25] Frey, S.; Heister, K.; Zharnikov, M.; Grunze, M. Modification of semifluorinated alkanethiolate monolayers by low energy electron irradiation. *Phys. Chem. Chem. Phys.* **2000**, *2*, 1979–1987.

[26] Chesneau, F.; Schüpbach, B.; Szelągowska-Kunstman, K.; Ballav, N.; Cyganik, P.; Terfort, A.; Zharnikov, M. Self-assembled monolayers of perfluoroterphenyl-substituted alkanethiols: Specific characteristics and odd-even effects. *Phys. Chem. Chem. Phys.* **2010**, *12*, 12123–12127.

[27] Moulder, J. F.; Stickle, W. E.; Sobol, P. E.; Bomben, K. D.

Handbook of X-Ray Photoelectron Spectroscopy; Perkin-Elmer Corporation: Eden Prairie, 1992.
[28] Stöhr, J. *NEXAFS Spectroscopy* (*Springer series in surface sciences*); Springer: Berlin, 2003.
[29] Batson, P. E. Carbon 1s near-edge-absorption fine structure in graphite. *Phys. Rev. B* **1993**, *48*, 2608–2610.
[30] Hermann, K.; Pettersson, L. G. M.; Casida, M. E.; Daul, C.; Goursot, A.; Koester, A.; Proynov, E.; St-Amant, A.; Salahub, D. R.; et al. StoBe-deMon, version 3.1, 2011.
[31] Perdew, J. P. Density-functional approximation for the correlation energy of the inhomogeneous electron gas. *Phys. Rev. B* **1986**, *33*, 8822–8824.
[32] Becke, A. D. Density-functional exchange-energy approximation with correct asymptotic behavior. *Phys. Rev. A* **1988**, *38*, 3098–3100.
[33] Perdew, J. P. Erratum: Density-functional approximation for the correlation energy of the inhomogeneous electron gas. *Phys. Rev. B* **1986**, *34*, 7406.
[34] Pettersson, L. G. M.; Wahlgren, U.; Gropen, O. Effective core potential parameters for first- and second-row atoms. *J. Chem. Phys.* **1987**, *86*, 2176–2184.
[35] Kutzelnigg, W.; Fleischer, U.; Schindler, M. The IGLO-method: *Ab-initio* calculation and interpretation of NMR chemical shifts and magnetic susceptibilities. In *Deuterium and Shift Calculation*. Fleischer, U.; Kutzelnigg, W.; Limbach, H. H.; Martin, G. J.; Martin, M. L.; Schindler, M., Eds.; Springer: Berlin, 1991; pp 165–262.
[36] Triguero, L.; Pettersson, L. G. M.; Ågren, H. Calculations of near-edge X-ray-absorption spectra of gas-phase and chemisorbed molecules by means of density-functional and transition-potential theory. *Phys. Rev. B* **1998**, *58*, 8097–8110.
[37] Weigend, F. Accurate coulomb-fitting basis sets for H to Rn. *Phys. Chem. Chem. Phys.* **2006**, *8*, 1057–1065.
[38] Neese, F.; Wennmohs, F.; Becker, U.; Riplinger, C. The ORCA quantum chemistry program package. *J. Chem. Phys.* **2020**, *152*, 224108.
[39] Cabarcos, O. M.; Schuster, S.; Hehn, I.; Zhang, P. P.; Maitani, M. M.; Sullivan, N.; Giguère, J. B.; Morin, J. F.; Weiss, P. S.; Zojer, E. et al. Effects of embedded dipole layers on electrostatic properties of alkanethiolate self-assembled monolayers. *J. Phys. Chem. C* **2017**, *121*, 15815–15830.
[40] Piserchia, A.; Zerbetto, M.; Salvia, M. V.; Salassa, G.; Gabrielli, L.; Mancin, F.; Rastrelli, F.; Frezzato, D. Conformational mobility in monolayer-protected nanoparticles: From torsional free energy profiles to NMR relaxation. *J. Phys. Chem. C* **2015**, *119*, 20100–20110.
[41] Zharnikov, M. High-resolution X-ray photoelectron spectroscopy in studies of self-assembled organic monolayers. *J. Electron Spectrosc. Relat. Phenom.* **2010**, *178–179*, 380–393.
[42] Ratner, B. D.; Castner, D. G. Electron spectroscopy for chemical analysis. In *Surface Analysis—The Principal Techniques*. Vickerman, J., Ed.; Wiley: Chichester, 1997.
[43] Heister, K.; Johansson, L. S. O.; Grunze, M.; Zharnikov, M. A detailed analysis of the C 1s photoemission of n-alkanethiolate films on noble metal substrates. *Surf. Sci.* **2003**, *529*, 36–46.
[44] Asyuda, A.; Das, S.; Zharnikov, M. Thermal stability of alkanethiolate and aromatic thiolate self-assembled monolayers on Au(111): An X-ray photoelectron spectroscopy study. *J. Phys. Chem. C* **2021**, *125*, 21754–21763.
[45] Lamont, C. L. A.; Wilkes, J. Attenuation length of electrons in self-assembled monolayers of n-alkanethiols on gold. *Langmuir* **1999**, *15*, 2037–2042.
[46] Schreiber, F. Structure and growth of self-assembling monolayers. *Prog. Surf. Sci.* **2000**, *65*, 151–256.
[47] Zharnikov, M.; Frey, S.; Rong, H.; Yang, Y. J.; Heister, K.; Buck, M.; Grunze, M. The effect of sulfur–metal bonding on the structure of self-assembled monolayers. *Phys. Chem. Chem. Phys.* **2000**, *2*, 3359–3362.
[48] Lee, S.; Puck, A.; Graupe, M.; Colorado, R.; Shon, Y. S.; Lee, T. R.; Perry, S. S. Structure, wettability, and frictional properties of phenyl-terminated self-assembled monolayers on gold. *Langmuir* **2001**, *17*, 7364–7370.
[49] Rong, H. T.; Frey, S.; Yang, Y. J.; Zharnikov, M.; Buck, M.; Wühn, M.; Wöll, C.; Helmchen, G. On the importance of the headgroup substrate bond in thiol monolayers: A study of biphenyl-based thiols on gold and silver. *Langmuir* **2001**, *17*, 1582–1593.
[50] Cyganik, P.; Buck, M.; Azzam, W.; Wöll, C. Self-assembled monolayers of ω-biphenylalkanethiols on Au(111): Influence of spacer chain on molecular packing. *J. Phys. Chem. B* **2004**, *108*, 4989–4996.
[51] Tao, F.; Bernasek, S. L. Understanding odd-even effects in organic self-assembled monolayers. *Chem. Rev.* **2007**, *107*, 1408–1453.
[52] Bagus, P. S.; Weiss, K.; Schertel, A.; Wöll, C.; Braun, W.; Hellwig, C.; Jung, C. Identification of transitions into Rydberg states in the X-ray absorption spectra of condensed long-chain alkanes. *Chem. Phys. Lett.* **1996**, *248*, 129–135.
[53] Väterlein, P.; Fink, R.; Umbach, E.; Wurth, W. Analysis of the X-ray absorption spectra of linear saturated hydrocarbons using the Xα scattered-wave method. *J. Chem. Phys.* **1998**, *108*, 3313–3320.
[54] Weiss, K.; Bagus, P. S.; Wöll, C. Rydberg transitions in X-ray absorption spectroscopy of alkanes: The importance of matrix effects. *J. Chem. Phys.* **1999**, *111*, 6834–6845.
[55] Schöll, A.; Fink, R.; Umbach, E.; Mitchell, G. E.; Urquhart, S. G.; Ade, H. Towards a detailed understanding of the NEXAFS spectra of bulk polyethylene copolymers and related alkanes. *Chem. Phys. Lett.* **2003**, *370*, 834–841.
[56] Perera, S. D.; Shokatian, S.; Wang, J.; Urquhart, S. G. Temperature dependence in the NEXAFS spectra of n-alkanes. *J. Phys. Chem. A* **2018**, *122*, 9512–9517.
[57] Shokatian, S.; Urquhart, S. Near edge X-ray absorption fine structure spectra of linear n-alkanes: Variation with chain length. *J. Electron Spectrosc. Relat. Phenom.* **2019**, *236*, 18–26.
[58] Feulner, P.; Zharnikov, M. High-resolution X-ray absorption spectroscopy of alkanethiolate self-assembled monolayers on Au(111) and Ag(111). *J. Electron Spectrosc. Relat. Phenom.* **2021**, *248*, 147057.
[59] Zharnikov, M.; Küller, A.; Shaporenko, A.; Schmidt, E.; Eck, W. Aromatic self-assembled monolayers on hydrogenated silicon. *Langmuir* **2003**, *19*, 4682–4687.
[60] Zharnikov, M.; Frey, S.; Heister, K.; Grunze, M. Modification of alkanethiolate monolayers by low energy electron irradiation: Dependence on the substrate material and on the length and isotopic composition of the alkyl chains. *Langmuir* **2000**, *16*, 2697–2705.
[61] Hähner, G.; Kinzler, M.; Thümmler, C.; Wöll, C.; Grunze, M. Structure of self-organizing organic films: A near edge X-ray absorption fine structure investigation of thiol layers adsorbed on gold. *J. Vac. Sci. Technol. A* **1992**, *10*, 2758–2763.
[62] Greenler, R. G. Infrared study of adsorbed molecules on metal surfaces by reflection techniques. *J. Chem. Phys.* **1966**, *44*, 310–315.
[63] Pearce, H. A.; Sheppard, N. Possible importance of a "metal-surface selection rule" in the interpretation of the infrared spectra of molecules adsorbed on particulate metals; infrared spectra from ethylene chemisorbed on silica-supported metal catalysts. *Surf. Sci.* **1976**, *59*, 205–217.
[64] Snyder, R. G.; Strauss, H. L.; Elliger, C. A. Carbon−hydrogen stretching modes and the structure of n-alkyl chains. 1. Long, disordered chains. *J. Phys. Chem.* **1982**, *86*, 5145–5150.
[65] MacPhail, R. A.; Strauss, H. L.; Snyder, R. G.; Elliger, C. A. Carbon-hydrogen stretching modes and the structure of n-alkyl chains. 2. Long, all-trans chains. *J. Phys. Chem.* **1984**, *88*, 334–341.
[66] Colorado, R.; Lee, T. R. Wettabilities of self-assembled monolayers on gold generated from progressively fluorinated alkanethiols. *Langmuir* **2003**, *19*, 3288–3296.
[67] Yu, T. L.; Marquez, M. D.; Zenasni, O.; Lee, T. R. Mimicking polymer surfaces using cyclohexyl- and perfluorocyclohexyl-terminated self-assembled monolayers. *ACS Appl. Nano Mater.* **2019**, *2*, 5809–5816.
[68] Gärtner, M.; Sauter, E.; Nascimbeni, G.; Petritz, A.; Wiesner, A.; Kind, M.; Abu-Husein, T.; Bolte, M.; Stadlober, B.; Zojer, E. et al. Understanding the properties of tailor-made self-assembled monolayers with embedded dipole moments for interface engineering. *J. Phys. Chem. C* **2018**, *122*, 28757–28774.
[69] Kang, J. F.; Ulman, A.; Liao, S.; Jordan, R.; Yang, G. H.; Liu, G. Y. Self-assembled rigid monolayers of 4 ′-substituted-4-mercapto-

biphenyls on gold and silver surfaces. *Langmuir* **2001**, *17*, 95–106.
[70] Yu, T. L.; Marquez, M. D.; Lee, T. R. SAMs on gold derived from adsorbates having phenyl and cyclohexyl tail groups mixed with their phase-incompatible fluorinated analogues. *Langmuir* **2022**, *38*, 13488–13496.
[71] Rodil, A.; Bosisio, S.; Ayoup, M. S.; Quinn, L.; Cordes, D. B.; Slawin, A. M. Z.; Murphy, C. D.; Michel, J.; O'Hagan, D. Metabolism and hydrophilicity of the polarised 'Janus face' all-*cis* tetrafluorocyclohexyl ring, a candidate motif for drug discovery. *Chem. Sci.* **2018**, *9*, 3023–3028.
[72] Benneckendorf, F. S.; Hillebrandt, S.; Ullrich, F.; Rohnacher, V.; Hietzschold, S.; Jänsch, D.; Freudenberg, J.; Beck, S.; Mankel, E.; Jaegermann, W. et al. Structure–property relationship of phenylene-based self-assembled monolayers for record low work function of indium tin oxide. *J. Phys. Chem. Lett.* **2018**, *9*, 3731–3737.
[73] Derry, G. N.; Kern, M. E.; Worth, E. H. Recommended values of clean metal surface work functions. *J. Vac. Sci. Technol. A* **2015**, *33*, 060801.
[74] Ford, W. E.; Gao, D. Q.; Knorr, N.; Wirtz, R.; Scholz, F.; Karipidou, Z.; Ogasawara, K.; Rosselli, S.; Rodin, V.; Nelles, G. et al. Organic dipole layers for ultralow work function electrodes. *ACS Nano* **2014**, *8*, 9173–9180.
[75] Alloway, D. M.; Hofmann, M.; Smith, D. L.; Gruhn, N. E.; Graham, A. L.; Colorado, R. Jr.; Wysocki, V. H.; Lee, T. R.; Lee, P. A.; Armstrong, N. R. Interface dipoles arising from self-assembled monolayers on gold: UV-photoemission studies of alkanethiols and partially fluorinated alkanethiols. *J. Phys. Chem. B* **2003**, *107*, 11690–11699.
[76] Boudinet, D.; Benwadih, M.; Qi, Y. B.; Altazin, S.; Verilhac, J. M.; Kroger, M.; Serbutoviez, C.; Gwoziecki, R.; Coppard, R.; Le Blevennec, G. et al. Modification of gold source and drain electrodes by self-assembled monolayer in staggered n- and p-channel organic thin film transistors. *Org. Electron.* **2010**, *11*, 227–237.
[77] Lee, H. J.; Jamison, A. C.; Lee, T. R. Surface dipoles: A growing body of evidence supports their impact and importance. *Acc. Chem. Res.* **2015**, *48*, 3007–3015.
[78] Zenasni, O.; Marquez, M. D.; Jamison, A. C.; Lee, H. J.; Czader, A.; Lee, T. R. Inverted surface dipoles in fluorinated self-assembled monolayers. *Chem. Mater.* **2015**, *27*, 7433–7446.
[79] Pratik, S. M.; Nijamudheen, A.; Datta, A. Janus all-*cis*-1, 2, 3, 4, 5, 6-hexafluorocyclohexane: A molecular motif for aggregation-induced enhanced polarization. *ChemPhysChem* **2016**, *17*, 2373–2381.
[80] Schlenoff, J. B.; Li, M.; Ly, H. Stability and self-exchange in alkanethiol monolayers. *J. Am. Chem. Soc.* **1995**, *117*, 12528–12536.
[81] Dauselt, J.; Zhao, J. L.; Kind, M.; Binder, R.; Bashir, A.; Terfort, A.; Zharnikov, M. Compensation of the odd-even effects in araliphatic self-assembled monolayers by nonsymmetric attachment of the aromatic part. *J. Phys. Chem. C* **2011**, *115*, 2841–2854.